



# In situ cosmogenic $^3\text{He}$ and $^{36}\text{Cl}$ and radiocarbon dating of volcanic deposits refine the Pleistocene and Holocene eruption chronology of SW Peru

Gordon R. M. Bromley<sup>1,2</sup> · Jean-Claude Thouret<sup>3</sup> · Irene Schimmelpfennig<sup>4</sup> · Jersy Mariño<sup>5</sup> · David Valdivia<sup>5</sup> · Kurt Rademaker<sup>6</sup> · Socorro del Pilar Vivanco Lopez<sup>7</sup> · ASTER Team<sup>4</sup> · Georges Aumaître · Didier Bourlès · Karim Keddadouche

Received: 30 March 2019 / Accepted: 6 September 2019

© International Association of Volcanology & Chemistry of the Earth's Interior 2019

## Abstract

Constraining the age of young lavas, which generally fall outside the effective range of traditional geochronology methods, remains a key challenge in volcanology, limiting the development of high-resolution eruption chronologies. We present an in situ cosmogenic  $^3\text{He}$  and  $^{36}\text{Cl}$  surface-exposure chronology, alongside new minimum-limiting  $^{14}\text{C}$  ages, documenting young eruptions at five sites in the Western Cordillera, southern Peru. Four  $^3\text{He}$ -dated lavas on the Nevado Coropuna volcanic complex (hitherto thought to be dormant) indicate that the central dome cluster is young and potentially active; two Holocene lavas on the easternmost dome are the youngest directly dated lavas in Peru to date. East of Coropuna, lava domes and block-lava flows represent the most extensive output to date of Nevado Sabancaya, one of Peru's most active volcanoes. Two  $^3\text{He}$  measurements confirm the Holocene age of these deposits and expand the chronology for one of the youngest major lava fields in Peru.  $^{36}\text{Cl}$  surface-exposure ages from the Purupurini dome cluster and Nevado Casiri document middle-late-Holocene episodes of effusive activity, while basal  $^{14}\text{C}$  ages from a lava-dammed wetland constrain an effusive eruption at Mina Arcata, north of Coropuna, to the late-glacial period. These new data advance the recent Western Cordillera volcanic record whilst demonstrating both the considerable potential and fundamental limitations of cosmogenic surface-exposure methods for such applications.

**Keywords** Cosmogenic surface-exposure dating · Helium-3 · Chlorine-36 · Lava flows ·  $^{14}\text{C}$  dating · Peruvian Andes

---

Editorial responsibility: H. Dieterich; Deputy Executive Editor: J. Tadeucci

**Electronic supplementary material** The online version of this article (<https://doi.org/10.1007/s00445-019-1325-6>) contains supplementary material, which is available to authorized users.

✉ Gordon R. M. Bromley  
gordon.bromley@nuigalway.ie

<sup>1</sup> School of Geography, Archaeology and Irish Studies, NUI Galway, Galway, Ireland

<sup>2</sup> Climate Change Institute, University of Maine, Orono, ME, USA

<sup>3</sup> Université Clermont Auvergne, Laboratoire Magmas et Volcans UMR 6524 CNRS and IRD R163, OPGC, Campus Universitaire des Cézeaux, 6 Avenue Blaise Pascal, TSA 60026-CS 60026, 63178 Aubière Cedex, France

<sup>4</sup> CNRS, INRA, IRD, Coll de France, CEREGE, Aix-Marseille Université, Aix en Provence, France

<sup>5</sup> Observatorio Vulcanológico del INGEMMET, OVI Instituto Geológico Minero y Metalúrgico, Arequipa, Peru

<sup>6</sup> Department of Anthropology, Michigan State University, Lansing, MI, USA

<sup>7</sup> Instituto Geofísico del Peru, Lima, Peru

## Introduction

As the dynamic interface between our planet's interior and exterior, volcanism plays a fundamental role in shaping Earth's surface morphology and atmosphere and, ultimately, human activity. Determining the timing and frequency of past eruptions therefore is central to understanding the processes driving volcanism and projecting future volcanic behaviour and associated geohazards (Andronico and Lodato 2005; Siebe et al. 2005; Gehrels et al. 2006; Huybers and Langmuir 2009; Molloy et al. 2009; Alcalá-Reygosa et al. 2018). Establishing detailed eruption chronologies also lays the requisite foundation for quantifying rates of magma production (Francis and Hawkesworth 1994) and landscape evolution, establishing the role of volcanism in past human and environmental change (Lentfer and Torrence 2007), and exploring links between external factors, most notably cryospheric change, and magma chamber dynamics (Harðarson and Fitton 1991; Nowell et al. 2006; Huybers and Langmuir 2009). Indeed, previous investigations into glacial-magmatic relationships have highlighted decompression melting (Harðarson and Fitton 1991; Maclennan et al. 2002; Pagli and Sigvaldson 2008) and reduced confining pressure on the magma chamber (Hall 1982; Hooper et al. 2011) as plausible consequences of rapid deglaciation. Such processes are particularly relevant in high-elevation volcanic regions such as the tropical Andes of South America, which in recent decades have experienced some of the highest rates of atmospheric warming and deglaciation on the planet (Mark and Seltzer 2005; Vuille et al. 2008). Yet, comprehensive eruption chronologies require accurate and precise dating of volcanic deposits, many of which are too young to be constrained with traditional methods.

The tropical Andes are an ideal location for investigating cryospheric-volcanic links owing to the abundance of high-elevation, active and dormant volcanic edifices with clear and well-preserved evidence for glaciation during the Late Pleistocene. To date, the majority of tropical Andean eruption chronologies employ indirect age constraint of volcanic landforms. Tephra deposits and lava flows, for example, are commonly dated by  $^{14}\text{C}$  ages of predating and/or overlying organic material or via stratigraphic relationships with adjacent deposits (e.g., Thouret et al., 1990, 1995a, 2001a; Gerbe and Thouret 2004; Delacour et al. 2007). In southern Peru, which is the focus of our study,  $^{14}\text{C}$ -dated tephra deposits have been employed with geochemical fingerprinting to establish the timing and likely source of prehistoric eruptions (Juvigné et al. 1997, 2008; Thouret et al. 2001b, 2005; Cobeñas et al. 2014). While these approaches afford valuable first-order constraints, each is limited by the robustness of stratigraphic correlation and the potentially broad bracketing timeframes involved.

In contrast, more direct assessments of eruption age include K-Ar,  $^{40}\text{Ar}/^{39}\text{Ar}$ , and surface-exposure methods. In southern Peru, Weibel et al. (1978) used K-Ar and Thouret et al. (2016,

2017) used  $^{40}\text{Ar}/^{39}\text{Ar}$  and U/Pb to date ignimbrites and lavas around Nevado Coropuna, whereas Samaniego et al. (2016) presented an extensive K-Ar data set constraining past eruptions of the Ampato-Sabancaya massif. Across the Peruvian–Chilean border, Wörner et al. (2000) applied  $^{40}\text{Ar}/^{39}\text{Ar}$  and K-Ar dating to Cenozoic deposits in northern Chile, while Hora et al. (2007) employed  $^{40}\text{Ar}/^{39}\text{Ar}$  to establish the Volcán Parinacota eruption record. Finally, the ongoing refinement of cosmogenic surface-exposure dating using in situ cosmogenic helium-3 and chlorine-36 (hereafter  $^3\text{He}$  and  $^{36}\text{Cl}$ ) has opened new opportunities for dating lavas directly and with increasing accuracy and precision (Blard et al. 2013; Schimmelpfennig et al. 2009, 2011). However, thus far,  $^3\text{He}$  and  $^{36}\text{Cl}$  dating of volcanic deposits in the tropical Andes has been applied to only a handful of lava flows in southern Peru (Samaniego et al. 2016; Úbeda et al. 2012, 2018) and northern Chile (Wörner et al. 2000) and the efficacy of these methods for constraining young (e.g., Holocene) lavas has not been tested rigorously.

Motivated by the need to assess the viability of cosmogenic nuclides for dating volcanic deposits on various timescales, we report a suite of new lava ages, constrained with  $^3\text{He}$  and  $^{36}\text{Cl}$  measurements in pyroxene and feldspar, respectively, for four volcanoes of the Pleistocene-age Frontal Arc in southern Peru's Western Cordillera: the Nevado Coropuna volcanic complex, Ampato-Sabancaya massif, Nevado Casiri, and Purupurini dome complex (Fig. 1). Together, these data (i) confirm the suitability of the cosmogenic  $^3\text{He}$  and  $^{36}\text{Cl}$  methods for dating lavas as young as  $< 2$  ka and (ii) expand the eruptive history of this sector of the Central Volcanic Zone (CVZ), information that lays the foundation for refining regional hazard assessments and exploring the relationships (if any) between cryospheric change and volcanism. Additionally, we describe new minimum-limiting  $^{14}\text{C}$  ages from a young lava flow at Arcata (MA) (Fig. 1),  $\sim 70$  km NNE of Nevado Coropuna, that potentially represents the most recent activity of the Arcata caldera and affords a new calibration for the in situ production of cosmogenic beryllium-10. Such calibration is crucial for improving the accuracy of cosmogenic surface-exposure dating.

## Geologic setting

As part of the CVZ ( $14\text{--}27^\circ\text{S}$ ), the Western Cordillera ( $\sim 15^\circ\text{S}$ ; Fig. 1) is the product of high-angle subduction of the Nazca Plate beneath the South American Plate (Dorbath 1996; Stern 2004). Currently, subduction along this boundary occurs at  $7\text{--}9$  cm/yr (Stern 2004), augmenting the considerable crust thickness ( $\sim 70$  km; James 1971) underlying the CVZ and resulting in widespread volcanism. The topographic expression of this volcanism is the  $> 3$  km-high Oligo-Miocene ignimbrite Altiplano-Puna Volcanic Complex (northern Chile and SW Bolivia) and Arequipa domain (southern Peru; Wörner et al. 2018), upon which has formed a suite of

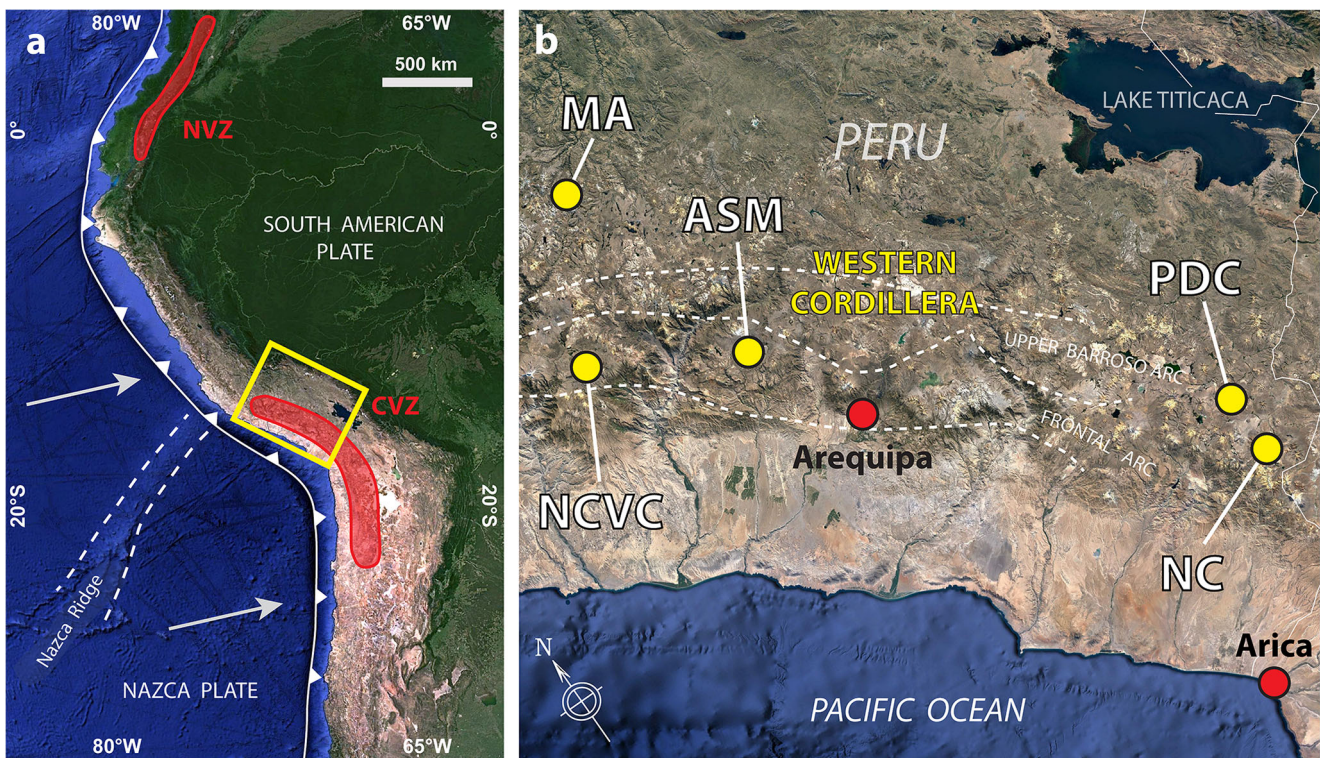


**Fig. 1** **a** Locations of the Central Volcanic Zone (CVZ) and Northern Volcanic Zone (NVZ) and the general tectonic context. Yellow square depicts area covered in panel **b**. **b** Location of our five study sites. Approximate positions of the Frontal Arc adapted from Gunnell et al. (2010)

Quaternary–Holocene composite volcanoes, caldera systems, and monogenetic fields (Baker 1981; Allmendinger et al. 1997). Due to their great elevation, many composite volcanoes, including Nevados Coropuna (6377 m), Solimana (6093 m), and Ampato (6288 m), currently support glaciers and snow fields. Coupled with the region’s large agricultural and urban populations (> 800,000 people live in the city of Arequipa, at the base of Volcán Misti), this combination of widespread volcanism and extensive cryosphere render the Western Cordillera a priority area for assessing future volcanic hazards and highlights the growing need for high-resolution, directly dated eruption chronologies on all time scales.

**Nevado Coropuna** The Nevado Coropuna volcanic complex (NCVC) ( $-15.5526^{\circ}$ ,  $-72.6348^{\circ}$ , 6377 m; Fig. 1) roughly parallels the Andean N120°-striking faults, along which are located most of the high, sprawling composite volcanoes forming the Frontal Arc in SW Peru. Comprising a series of eroded composite volcanoes crowned by five youthful, high-relief (up to 3000 m relief above the surrounding plateau) glaciated lava domes, the NCVC exhibits three fresh-looking lavas (Fig. 2a) and numerous older flows, the latter underlying moraines of the last glacial maximum (LGM,  $\sim 20$  ka; Forget et al. 2008; Bromley et al. 2009). Until recently, the NCVC has widely been thought to be dormant. Previous tephrostratigraphy work at the NCVC identified a period of activity at 27–37 ka (Thouret et al.

2003), while Úbeda et al. (2012, 2018) reported Holocene ages for the three young lavas based on whole-rock  $^{36}\text{Cl}$  (Fig. 3). The landforms sampled in this study are block-lava flows of andesitic composition ( $\text{SiO}_2$  56–62 wt.%; Venturelli et al. 1978).

**Ampato–Sabancaya** The Ampato–Sabancaya massif (ASM) ( $-15.818^{\circ}$ ,  $-71.8778^{\circ}$ ; Fig. 1) is separated from the NCVC by the Río Colca canyon. Together, Ampato (6288 m) and Sabancaya (5992 m) form the southern half of a 20 km-long volcanic massif terminating to the north in the older and severely eroded Nevado Hualca Hualca edifice (6025 m). Today, Ampato nourishes a small ( $\sim 2$  km<sup>2</sup>) summit glacier; however, relict moraines (Alcalá et al. 2011) indicate this glacier was significantly larger during the LGM. According to Samaniego et al. (2016), Ampato’s basal edifice dates to 450 ka and the upper structure and summit cone to  $\sim 200$ –230 ka and 20–10 ka, respectively. Subsequent northward vent migration resulted in the construction of Nevado Sabancaya (Figs. 2b and 4), which is characterized by an extensive field of andesitic–dacitic ( $\text{SiO}_2$  60–66 wt.%; Samaniego et al. 2016) stubby block-lava flows (Thouret et al. 1994, 1995b; Samaniego et al. 2016). Between 1990 and 1998, Sabancaya underwent a period of explosive volcanism detailed by Gerbe and Thouret (2004). Moderate explosive activity resumed in November 2016 and is ongoing at the time of writing.

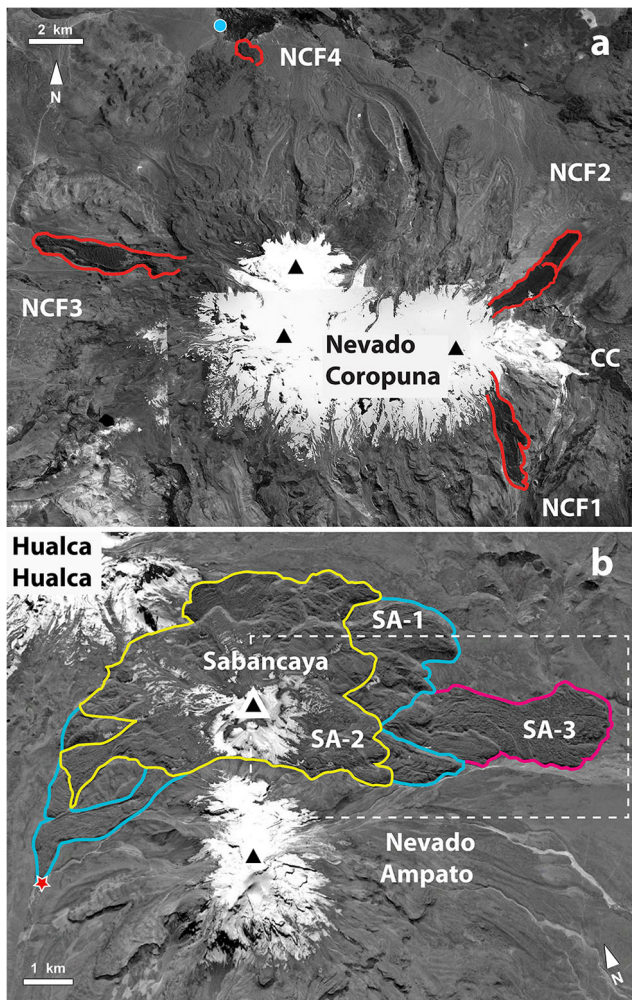


**Fig. 2** Distribution of studied lava flows on the NCVC **a** and ASM **b**. Blue circle and ‘CC’ in panel **a** indicate Mauca Llacta and Cerro Cuncaicha, respectively. The different colours in panel **b** distinguish overlapping lavas of different ages (adapted from Samaniego et al. 2016). Red star in panel **b** marks the location of a maximum-limiting  $^{14}\text{C}$  age ( $5540 \pm 40$  cal yr) for the basal lava (Thouret et al. 2001a), while the dashed white line indicates the area covered in detail in Fig. 4

**Purupurini** The Purupurini dome complex (PDC) ( $-17.291^\circ$ ,  $-69.889^\circ$ , 5117 m; Fig. 1) comprises a group of prominent dacitic ( $\text{SiO}_2$  66 wt.%) lava domes and dome coulees located  $\sim 270$  km ESE of the ASM and 85 km NNE of the city of Tacna. Figure 5 depicts four voluminous lava domes 3.5–7 km<sup>2</sup> in area and six smaller ( $< 0.5$  km<sup>2</sup> area) intrusions, situated in the NE corner of a large depression surrounded by eroded composite Quaternary volcanoes (Fig. S1). The arcuate rim of the depression, which opens to the north-east, suggests the former existence of a 13 km-diameter caldera, the northern edge of which is the site of the recent extrusions (Fig. S1). With the exception of the E–W-oriented middle dome, the Purupurini domes are elongated in a NNE direction (Fig. S1). Crosscutting the dome cluster are three discrete populations of  $\text{N}05^\circ$  E-,  $\text{N}85^\circ$  E-, and  $\text{N}175^\circ$  E-striking faults (Fig. S1). The most voluminous dome coulee is elongated along the most

recent  $\text{N}00\text{--}05^\circ$  E strike-slip fault (Fig. S1). North of the largest dome coulee, a graben bounded by two  $\text{N}178^\circ$  E strike-slip and normal faults cuts the depression floor and the surrounding Holocene slope and fan deposits.

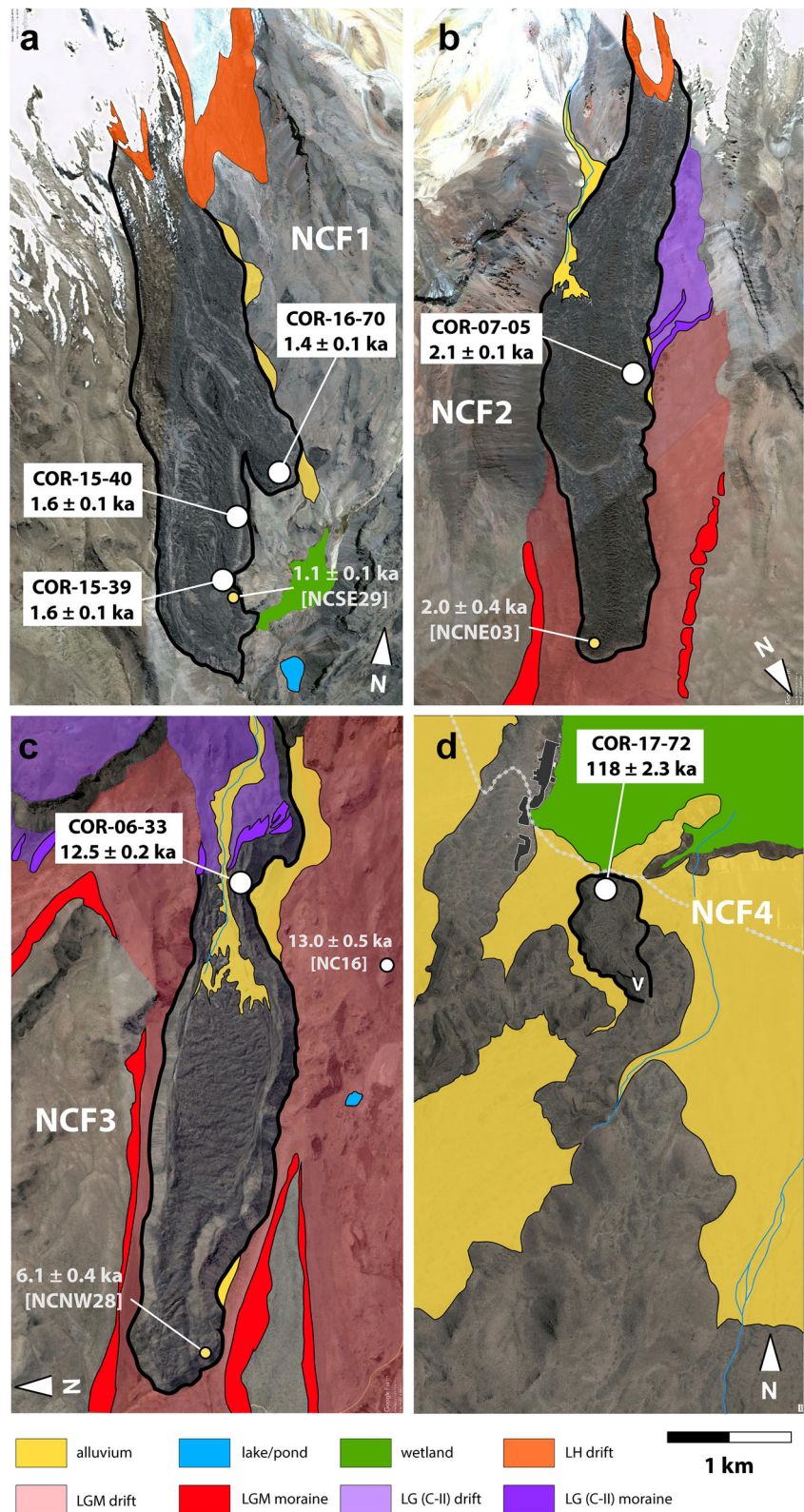
**Nevado Casiri** Adjacent the Peru–Chile border, Nevado Casiri (NC) ( $-17.485^\circ$ ,  $-69.789^\circ$ , 5328 m; Fig. 1) comprises a young complex of andesitic ( $\text{SiO}_2$  60%–61 wt.%) domes and lava flows overlying the southern flanks of hydrothermally altered Quaternary volcanoes (Fig. S2). The NC complex occupies a structural low—potentially a graben—bounded by  $\text{N}150^\circ$  E-striking faults and is surrounded by eroded composite volcanoes to the north, lava domes to the west, and a dome cluster to the east (Fig. S2). The summit vent of one of NC’s lava cones exhibits a conspicuous,  $\sim 100$  m-relief plug dome (Fig. 6). The vent itself has been breached to the south, probably due to dome collapse flows, as indicated by a thick apron of pyroclastic deposits on the slopes below. West of the vent is an extensive field of at least four stubby block-lava flows (Fig. 6).

**Mina Arcata** Seventy kilometres north of the NCVC, the Mina Arcata (MA) site ( $-14.999^\circ$ ,  $-72.365^\circ$ ,  $\sim 4860$  m; Fig. 1) comprises a blocky trachyandesite ( $\text{SiO}_2$  56 wt.%) lava flow, 3.5 km<sup>2</sup> in area, and 4.2 km long, that erupted from a vent located along a  $\text{N}10^\circ$  E fault associated with the Orcopampa hemi-graben. The vent is situated on the west wall of a south-flowing glacial valley, Quebrada Angostura, draining Cerro Ancojahua. The lava flow dammed local drainage and impounded shallow lakes and peatlands against its margins (Fig. 7). We include the Arcata lava flow in this paper due to (i) the prominence of this ‘glacial valley-fill type’ of effusive flow in the Western Cordillera, (ii) the apparently young age of this most recent lava of the Arcata caldera, and (iii) the potential for this landform to provide a calibration site for cosmogenic beryllium-10. To date, there have been no published descriptions of the MA lava flow and its origin remains unclear.

## Methodology

Lava flows were mapped from Google Earth imagery and field-surveyed to establish stratigraphic relationships and relative weathering conditions, collect elevation data, and identify suitable surfaces for surface-exposure dating. Lava composition dictates the appropriate cosmogenic nuclide for constraining eruption ages. Both the NCVC and ASM are dominated by calc-alkaline andesites and dacites, containing abundant clinopyroxene and orthopyroxene phenocrysts (Venturelli et al. 1978; Gerbe and Thouret 2004; Burkett 2008; Samaniego et al. 2016). Because these minerals retain helium at typical environmental temperatures, they are ideal

**Fig. 3** Annotated Google Earth images of the four NCVV lava flows: **a** NCF1, **b** NCF2, **c** NCF3, **d** NCF4. Also shown are the distributions of glacial and alluvial deposits adjacent each flow and sample sites for cosmogenic <sup>3</sup>He dating (note: pre-volcanic glacial deposits are not depicted for NCF1, where geomorphic mapping is incomplete). Panel **c** also shows the distribution of <sup>3</sup>He ages of glacial erratics published previously by Bromley et al. (2009) and recalculated here using the updated production rate and scaling scheme. Yellow dots indicate previously reported whole-rock <sup>36</sup>Cl ages (Úbeda et al. 2012, 2018)



targets for <sup>3</sup>He dating. Recent refinement of <sup>3</sup>He production rates at high tropical altitudes (Blard et al. 2013; Kelly et al. 2015; Martin et al. 2017) means effective <sup>3</sup>He eruption chronologies are now possible for Western Cordillera volcanoes.

In contrast, although our observations show the NC and PDC sites are generally andesitic–dacitic in composition, the pyroxene content in our samples is low while Ca-rich feldspar is abundant. Consequently, <sup>36</sup>Cl dating of the feldspars is the

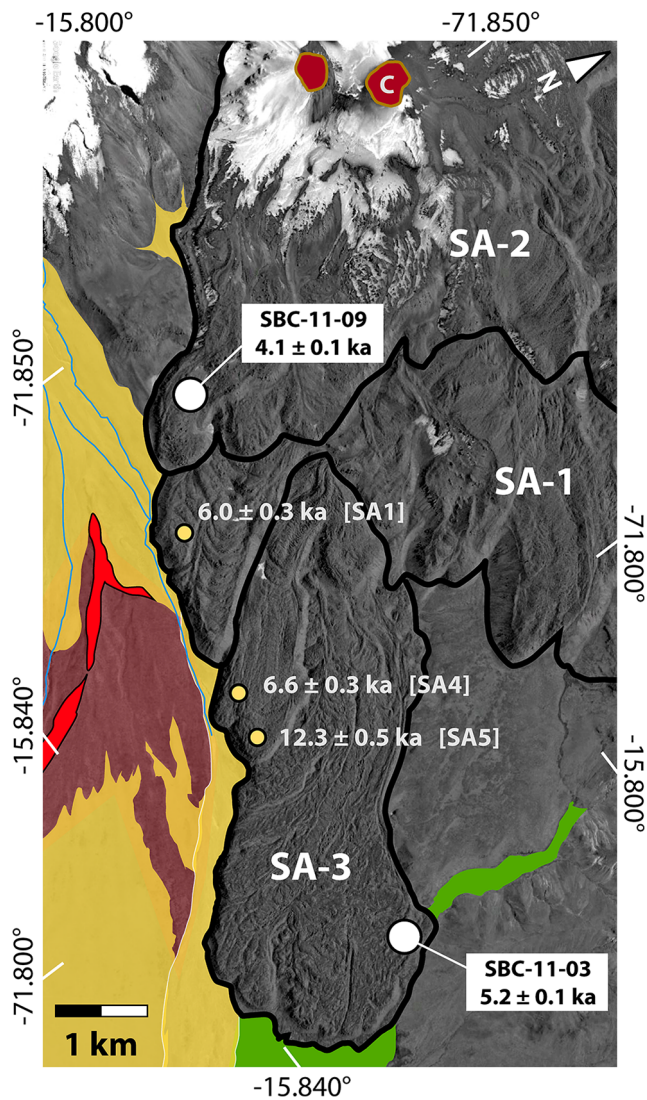


**Fig. 4** Annotated Google Earth image of the eastern flank of the ASM, showing units SA-1, SA-2, and SA-3 (after Samaniego et al. 2016) and sampling sites for cosmogenic <sup>36</sup>Cl dating. Also shown are the three ages published previously by Samaniego et al. (2016) and recalculated here using the same production rate and scaling scheme as our lava data. Sabancaya's craters ('C') are visible at the top of the image. Legend is as in Fig. 3

most suitable method to date these flows. Full details of sampling procedures and the preparation of pyroxenes for <sup>3</sup>He and feldspars for <sup>36</sup>Cl are given in Online Resource 1.

The semi-arid climate of the Western Cordillera (~390 mm/yr water equivalent at 6080 m on Coropuna; Herreros et al. 2009) underpins the application of surface-exposure dating at these sites by minimizing post-depositional rock-surface erosion and shielding by vegetation and snow. <sup>3</sup>He ages were calculated using the online University of Washington cosmogenic calculator v.3 (<https://hess.ess.washington.edu>) in conjunction with the Poccolli <sup>3</sup>He calibration data set (Blard et al. 2013) and time-independent 'St' scaling scheme (Lal 1991; Stone 2000) (Table 1). As

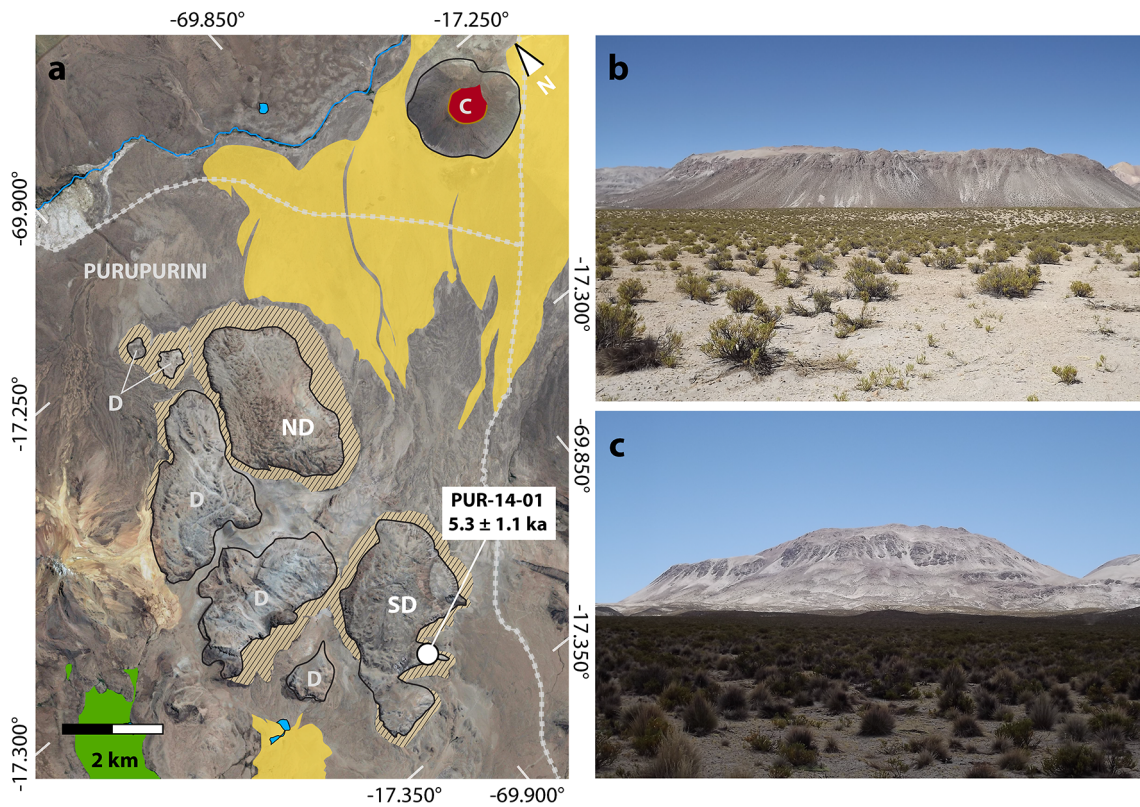
detailed in Online Resource 1, our interpretations are insensitive to scaling choice. All <sup>36</sup>Cl surface-exposure ages were calculated with the Excel® spreadsheet of Schimmelpfennig et al. (2009), employing the 'St' scaling scheme and incorporating <sup>36</sup>Cl production rates for spallation of Ca and K (Schimmelpfennig et al. 2011, 2014) and the production rate of epithermal neutrons from fast neutrons in the atmosphere at the land/atm interface (Marrero et al. 2016), which controls <sup>36</sup>Cl production by low-energy neutron capture on <sup>35</sup>Cl (see Online Resource 1). All relevant input data are provided in Tables 2 and 3; 1σ uncertainties of <sup>36</sup>Cl ages (Table 3) were determined through full propagation of analytical and production rate errors. Using the <sup>36</sup>Cl production rate for spallation of Ca calibrated by Marrero et al. (2016), which is ~20% higher than that of Schimmelpfennig et al. (2011), results in <sup>36</sup>Cl ages that are 2–11% younger (Table 3; see Online Resource 1), which is within the 1σ uncertainties of the <sup>36</sup>Cl ages and thus does not impact our conclusions.

In contrast to our other sites, the Arcata trachyandesite lava contains minimal pyroxene and only trace amounts of quartz. Therefore, we radiocarbon-dated organics preserved in the basal sediments of a lava-impounded wetland to provide first-order age constraint for the eruption, since the wetland would not have existed prior to the lava dam. We employed a Livingstone corer to extract a 4-m core from a small wetland adjacent the flow's eastern edge (−14.9985, −72.3603; 4763 m; Figs. 7 and 8), the surface of which is dominated by *Distichia muscoides* and fed by drainage from the surrounding slopes. The core was taken within 30 m distance of the lava edge and penetrated the full thickness of the palaeo-lacustrine sediments down to the underlying glacial diamicton (Fig. 8). The core was split at the University of Maine, where samples for <sup>14</sup>C dating (well-preserved remains of terrestrial plants) were isolated by sieving, cleaned in de-ionized water in an ultrasonic bath, dried, and submitted to the NOSAMS facility, Woods Hole Oceanographic Institute, for <sup>14</sup>C measurement. Radiocarbon dates were calibrated to calendar years using OxCal v.4.2 (Ramsey 2009) and IntCal13 (Table 4).

## Results

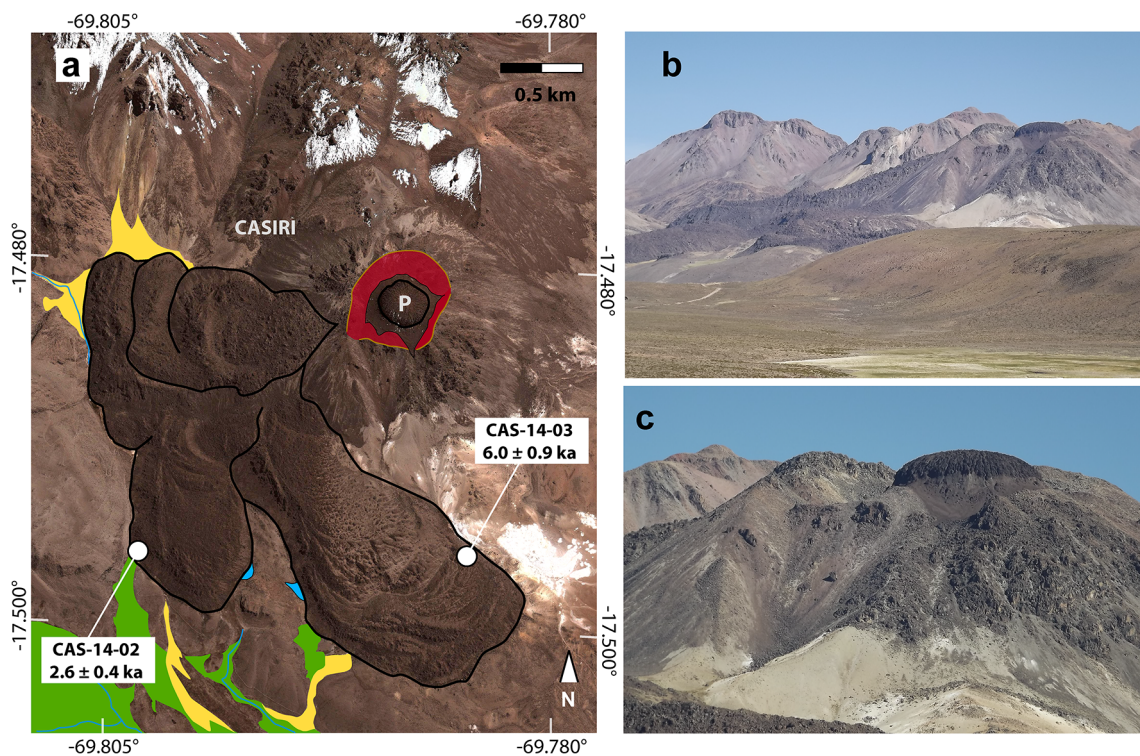
### Nevado Coropuna

Figure 2 a depicts the distribution of lava flows on the NCVC. The southern flow (NCF1), which erupted from the NCVC's east summit, is 4 km in length, 3.3 km<sup>2</sup> in area, and 50–150 m thick, and drops in elevation from 5510 m at the snowline to a terminus at 4250 m. The lava forms a single block-lava flow, indicating emplacement during a single event. The surface of NCF1 is relatively stable and fresh in appearance, exhibiting well-preserved glassy rinds, abundant high-relief and



**Fig. 5** Purupurini dome complex. **a** Annotated Google Earth image of the PDC site, showing the distributions volcanic and surficial deposits and sample site for cosmogenic  $^{36}\text{Cl}$  dating. ‘ND’ and ‘SD’ denote North

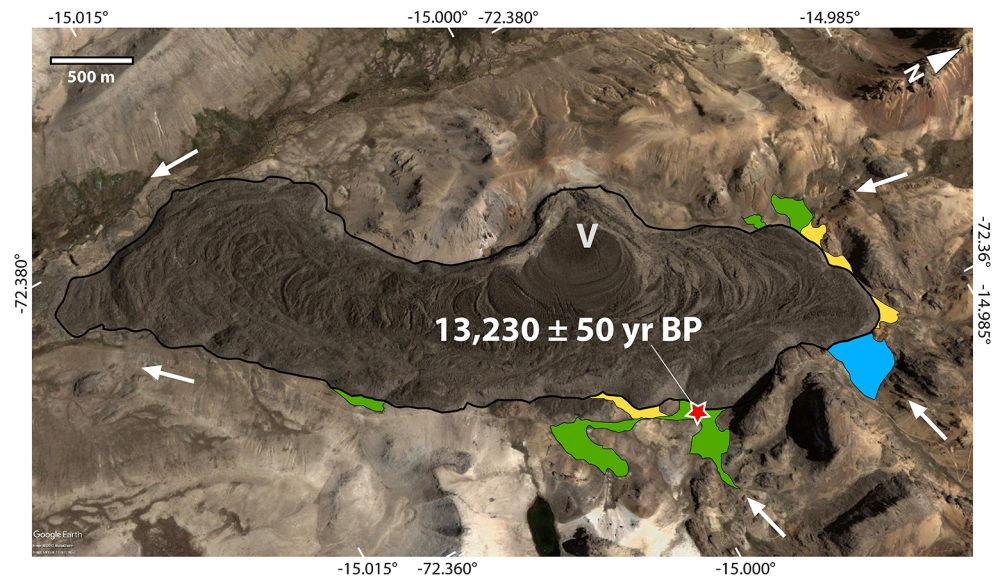
Dome and South Dome, respectively, while ‘D’ indicates minor dome structures and ‘C’ denotes crater. Photographs of the north **b** and south **c** lava domes. Legend is as in Fig. 3



**Fig. 6** Nevado Casiri complex. **a** Annotated Google Earth image of the NC site, showing the distributions volcanic and surficial deposits and sample sites for cosmogenic  $^{36}\text{Cl}$  dating. ‘P’ denotes summit plug

dome. **b** Photograph of the south-eastern flank of NC, showing part of the dated lava flow and the conspicuous summit plug dome. **c** Close-up view of the summit plug. Legend is as in Fig. 3

**Fig. 7** Annotated Google Earth image of the MA flow ('V' denotes vent), showing locations of lava-impounded ponds and wetlands and our core site (red star). Also shown is the average of two basal  $^{14}\text{C}$  ages from the core, which provide a minimum-limiting age for the eruption. Arrows denote general drainage directions of water in this catchment. Legend is as in Fig. 3



undisturbed pressure ridges, and minimal surface weathering. Stratigraphically, the flow overlies, and thus postdates, moraines of the LGM (Bromley et al. 2009). The upper flow has, in turn, been overrun by a small glacier tongue that deposited fresh, ice-cored moraines on the lava surface (Fig. 3a). Such moraines are widespread throughout the Western Cordillera and correlated with glacial advances during the last millennium (Forget et al. 2008; Bromley et al. 2011a; Alcalá-Reygosa et al. 2016). Three  $^3\text{He}$  samples (COR-15-39 and 40, COR-16-70; Table 1; Fig. 3a) collected from near the base of NCF1 are indistinguishable within  $2\sigma$  and give a mean exposure age of  $1545 \pm 90$  years.

On the northern flank of the eastern summit, NCF2 descends 700 m from its source at 5590 m to its terminus in

the U-shaped Queña Ranra valley (Fig. 3b). The 5 km-long flow has an area of  $3.6 \text{ km}^2$  and is weathered to a similar degree as NCF1. Stratigraphically, this flow overlies a late-glacial moraine dated in the adjoining valley to 13.4 ka (Bromley et al. [2011b], recalculated here using the same production rate and scaling). Like NCF1, the upper end of NCF2 has been glacially incised during a subsequent advance of the ice cap and is overlain by a fresh ice-cored moraine presumably of Late Holocene age (Clapperton 1993; Forget et al. 2013; Lamadon 1999) (Fig. 3b). Sample COR-07-05 gives a  $^3\text{He}$  age of  $2.1 \pm 0.1$  ka for this flow (Table 1; Fig. 3b).

The larger NCF3 flow was erupted from a vent or a WNW–ESE-striking fissure located between Coropuna's NW and SW domes (Fig. 2a). NCF3 is 6.25 km long, 50–100 m thick,

**Table 1** Sample data, helium concentrations, and surface-exposure ages for NCVC and ASM lava samples

Sample ID	Lat.	Long.	Altitude (m)	Thickness (cm)	Shielding	$^3\text{He}_{\text{cos}}$ ( $10^6 \text{ atoms g}^{-1}$ )	Exposure age and $1\sigma$ (ka) <sup>a</sup>
Flow NCF1							
COR-15-39	-15.595	-72.577	4300	3.0	0.998	$2.06 \pm 0.03$	$1.57 \pm 0.03$
COR-15-40	-15.592	-72.577	4450	4.0	0.998	$1.89 \pm 0.04$	$1.62 \pm 0.02$
COR-16-70	-15.588	-72.575	4630	3.0	0.998	$2.01 \pm 0.09$	$1.44 \pm 0.07$
Flow NCF2							
COR-07-05	-15.525	-72.569	5176	3.6	0.996	$3.66 \pm 0.11$	$2.10 \pm 0.07$
Flow NCF3							
COR-06-33	-15.518	-72.707	5024	4.0	0.999	$20.05 \pm 0.3$	$12.5 \pm 0.17$
Flow NCF4							
COR-17-72	-15.428	-72.673	4413	3.0	0.999	$149.0 \pm 2.9$	$118.2 \pm 2.3$
Flow SA2							
SBC-11-09	-15.816	-71.843	5076	2.8	0.999	$7.06 \pm 0.18$	$4.13 \pm 0.11$
Flow SA3							
SBC-11-03	-15.822	-71.785	4578	3.0	0.999	$7.15 \pm 0.18$	$5.18 \pm 0.13$

<sup>a</sup> Ages calculated assuming zero erosion and a density of  $2.75 \text{ g/cm}^3$

**Table 2** Sample locations and information required for  $^{36}\text{Cl}$  age calculations

Sample ID	Lat.	Long.	Altitude (m)	Density ( $\text{g}/\text{cm}^3$ )	Subsurface depth (cm) <sup>a</sup>	Thickness (cm)	Shielding	CaO% <sup>b</sup>	K <sub>2</sub> O % <sup>c</sup>	TiO <sub>2</sub> % <sup>d</sup>	Fe <sub>2</sub> O <sub>3</sub> % <sup>e</sup>
PUR-14-01	-17.329	-69.883	4826	2.5	7–5	2	0.950	5.19±0.10	1.63±0.03	0.06±0.01	0.42±0.02
CAS-14-02	-17.500	-69.801	4700	2.7	7–5	2	0.950	6.32±0.13	0.74±0.37	0	0.25±0.01
CAS-14-03	-17.500	-69.782	4750	2.7	7–5	2	0.950	6.27±0.13	0.72±0.04	0	0.24±0.01

<sup>a</sup> Sub-surface depth and sample depth are approximative (see text for details)

<sup>b–e</sup> Concentrations of the  $^{36}\text{Cl}$  target elements Ca, K, Ti and Fe were determined at the SARM-CRPG (Nancy, France) by ICP-OES (values of 0 denote measurements below detection limit)

covers an area of 4.5 km<sup>2</sup>, and ranges in elevation from 5140 m at its upper limit to 4596 m at the terminus. Like NCF1 and NCF2, NCF3 overlies LGM glacial till and is overlain in turn by moraines and glacio-fluvial outwash of a later, Holocene glacier advance (Fig. 3c). Yet, in contrast with, the overlying moraines at NCF3 are significantly older than those mantling NCF1 and NCF2, and instead resemble the late-glacial C-II moraines on the mountain's north side (Bromley et al. 2009, 2011b). Specifically, the overlying moraines exhibit broad crests and exfoliated boulder surfaces and lack the ice core characterising the Late Holocene moraines. Similarly, the lava flow itself is more weathered than NCF1 and NCF2, with a greater abundance of toppled crags and blocks, more widespread exfoliation of rock surfaces, and a thick (2–5 mm) weathering rind in hand specimens. A  $^3\text{He}$  exposure age from this flow indicates eruption at 12.5±0.2 ka (Table 1).

The fourth lava deposit examined here, NCF4, is a small (0.3 km<sup>2</sup>), steep-fronted porphyritic andesite flow erupted from a fissure located 1-km ESE of Mauca Llacta, at the base of Coropuna's NW dome (Fig. 2a). NCF4 has an altitude range of 4474–4400 m and is underlain by relict alluvial fans emanating from Coropuna; unlike the previous flows, NCF4 has not been influenced by glacial erosion. Morphologically, the lava exhibits clear flow structures, including levees and pressure ridges, while the fissure itself is also well preserved (Fig. 3d). Despite this well-preserved macromorphology, blocks comprising the surface of NCF4 exhibit extensive exfoliation, pitting, and well-developed weathering rinds, relative to flows NCF1–3, suggesting greater antiquity. A single sample, COR-17-72, collected from near the toe of the flow (Fig. 3d) gives a  $^3\text{He}$  age of 118±2.3 ka (Table 1).

### Ampato–Sabancaya massif

The volcanic landforms of the ASM has been mapped by Huaman-Rodrigo et al. (1993), Thouret et al. (1994, 1995b), Gerbe and Thouret (2004), Bulmer et al. (1999), and Samaniego et al. (2016), the latter who also provided three  $^3\text{He}$  measurements for lavas on the Sabancaya's eastern flank (see “Discussion”). Samaniego et al. (2016) described four separate east-flowing lava units and labelled these SA1–3,

for the basal lavas, and SA–4 for the most recent deposits (Figs. 2b and 4). Two of their  $^3\text{He}$  samples (SA4 and SA5) are from what they designated a satellite vent lava, flow SA-3, while the third sample, SA1, was collected from their ‘lower lava’ SA-1 (see below).

The excellent preservation of flow structures, levees, spines and crags, and absence of significant post-eruption weathering or glacial erosion are in keeping with the Holocene designation of Sabancaya's lavas. We measured helium concentrations in two samples. The first (SBC-11-03), from near the base of flow SA-3 of Samaniego et al. 2012, gives an age of 5.2±0.1 ka for that eruption (Fig. 4). The second sample, SBC-11-09, was collected from a higher and stratigraphically younger flow (SA-2 of Samaniego et al. 2012) and gives an age of 4.1±0.1 ka (Fig. 4).

### Purupurini dome cluster

A total of seven domes and dome coulees rise as much as 300 m above the former caldera floor at the PDC (Figs. 5 and S1). Without exception, the steep flanks and sub-horizontal dome surfaces are mantled by significant accumulations of wind-blown ash. Nonetheless, the prominent levees and bulges that are preserved atop each dome testify to the minimal impact of post-depositional weathering. Moreover, we note that, although relict moraines and glacial drift are widespread on the surrounding uplands, the PDC has not been impacted by glacial erosion. A single sample (PUR-14-01) collected from the top surface of the southern dome (Fig. 5) for cosmogenic  $^{36}\text{Cl}$  measurement yielded an exposure age of 5.3±1.1 ka (Table 3; Fig. 5).

### Nevado Casiri

The volcanic geomorphology of the NC volcano is illustrated in Figs. 6 and S2. Two prominent, minimally weathered block-lava flows, with a total area of ~3 km<sup>2</sup>, descend in a series of overlapping flow lobes from high (~5260 m) on the SW flank of the older main cone: the SW flow terminates at 4730 m elevation and the 2 km-long, stratigraphically older SE flow slightly higher at 4760 m (Fig. 6). Crowning the main

**Table 3**  $^{36}\text{Cl}$  ages for Purupurimi and Casiri samples and related analytical data

Sample ID	Weight (g)	Grain size fraction ( $\mu\text{m}$ )	Mass of Cl in spike (mg)	$^{35}\text{Cl}/^{37}\text{Cl}$	$^{36}\text{Cl}/^{35}\text{Cl}$ ( $10^{-4}$ )	[Cl] in sample (ppm)	$[\text{}^{36}\text{Cl}]$ ( $10^4$ atoms $\text{g}^{-1}$ )	Exposure age and $1\sigma$ (ka) ("Schimmelpfennig" production rates) <sup>a</sup>	Exposure age and $1\sigma$ (ka) ("Marrero" production rates) <sup>c</sup>
PUR-14-01	14.25	315–500	1.596	$4.372 \pm 0.04$	$16.51 \pm 0.65$	$374 \pm 21$	$110.4 \pm 6.3$	$5300 \pm 1100$	$5200 \pm 1100$
CAS-14-02	4.89	150–500	1.600	$78.07 \pm 0.95$	$2.17 \pm 0.20$	$15.9 \pm 0.9$	$10.2 \pm 1.3$	$2610 \pm 410$	$2320 \pm 370$
CAS-14-03	5.91	150–500	1.608	$20.24 \pm 0.19$	$7.09 \pm 0.47$	$64.3 \pm 3.3$	$37.0 \pm 2.6$	$5970 \pm 930$	$5540 \pm 830$
Blanks						Total atoms $^{36}\text{Cl}$ atoms Cl ( $10^{17}$ )			
BI.11.01.17	-	-	1.599	$590 \pm 16$	$0.447 \pm 0.081$	$6.91 \pm 0.63$	$12.3 \pm 2.2$		

<sup>a</sup> Ages calculated using  $^{36}\text{Cl}$  production rates for spallation of Ca and K calibrated by Schimmelpfennig et al. (2011, 2014). Samples were taken at  $\sim 5$  cm depth below the surface with a sample thickness of  $\sim 2$  cm (see Table 2 and text for details)

<sup>b</sup> Ages calculated using  $^{36}\text{Cl}$  production rates for spallation of Ca and K calibrated by Schimmelpfennig et al. (2011, 2014). Age calculations done assuming the samples were collected from the surface, with zero erosion, to demonstrate the effect of subsurface sampling on apparent exposure ages

<sup>c</sup> Ages calculated using  $^{36}\text{Cl}$  production rates for spallation of Ca and K calibrated by Marrero et al. (2016). Samples were taken at  $\sim 5$  cm depth below the surface with a sample thickness of  $\sim 2$  cm (see Table 2 and text for details)

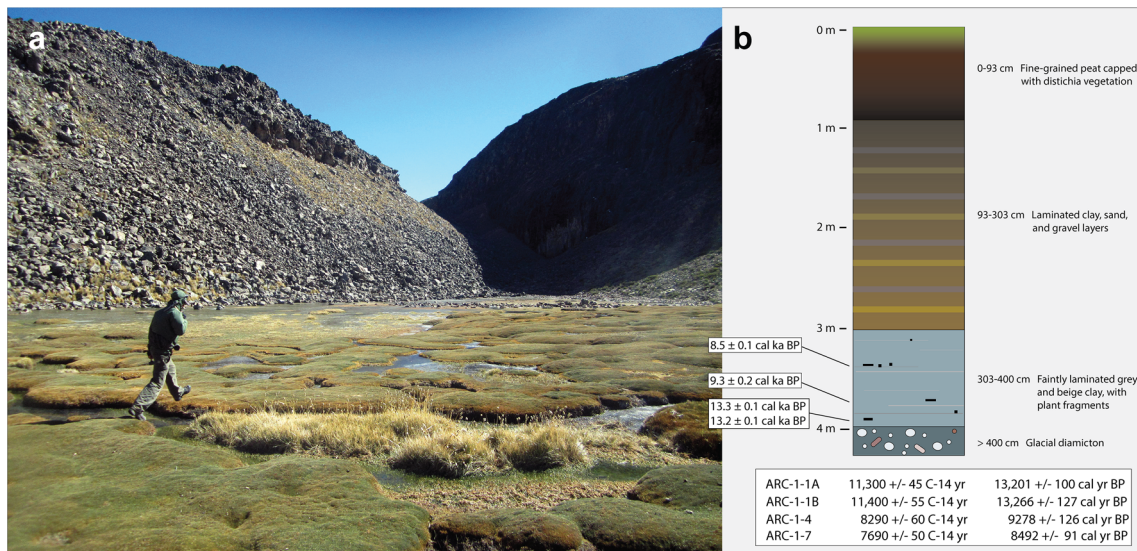


**Fig. 8** a Quebrada Angostura core site, showing the wetland in the foreground and the MA lava flow in the background. b Schematic diagram of the Arcata core and stratigraphic context of the four <sup>14</sup>C ages from plant macrofossils

cone, the striking protrusion (0.05 km<sup>2</sup>) forming the summit of NC is unweathered and its surface characterized by radial pressure ridges. Similarly, although the lower reaches of the southern lava are mantled by wind-blown ash, both flows exhibit a craggy topography including 50–100 m-tall levees and huge ropy lobes as much as 500-m wide, 130 m across, and 50-m tall. Nowhere do the lavas investigated here bear any evidence of glaciation. We collected one sample each from the upper surfaces of the two south-flowing lavas for cosmogenic <sup>36</sup>Cl dating. Sample CAS-14-02 gives an exposure age of 2.6 ± 0.4 ka for the stratigraphically younger flow, while CAS-14-03 has an age of 6.0 ± 0.9 ka (Table 3; Fig. 6).

**Mina Arcata**

The MA lava flow (Fig. 7) flowed both north and south from the vent along a NNE-trending fault. The surface of the flow, which stands up to 50 m above the adjacent valley floor, retains clear flow structures, including pressure ridges as much as 5 m in relief, and is similar in appearance to the andesitic block-lava flows on the NCVC and ASM. Nonetheless, the MA flow is visibly more weathered than the Holocene lavas described above, which potentially is due as much to the less-resistant trachyandesite lithology as

it is to age. Our sediment core reveals 97 cm of basal laminated grey-beige clay containing plant fragments, over which lie 210 cm of alternating sand-gravel lenses and grey clay, representing progressive infilling of the basin by alluvium, and an upper metre dominated by fine-grained peat transitioning into a fibrous distichia mat.

Four <sup>14</sup>C dates on plant material in the basal unit afford stratigraphically consistent minimum ages for the eruption (Fig. 8): ARCATA-1-1a and 1b, from 5 to 7 cm above the till-clay interface at ~395 cm depth, give calibrated ages (before AD 1950) of 13,200 ± 100 yr BP and 13,270 ± 130 yr, respectively (mean age 13,230 ± 50 yr BP); samples ARCATA-1-4 (370 cm depth) and ARCATA-1-7 (340 cm depth) give calibrated ages of 9280 ± 190 yr BP and 8490 ± 90 yr BP, respectively (Table 4).

**Discussion**

This paper presents eleven new <sup>3</sup>He and <sup>36</sup>Cl surface-exposure ages and <sup>14</sup>C data, which together expand the recent eruptive chronology of four composite volcanoes and one minor vent in the CVZ. At the NCVC, our data provide the first constraint of an eruption at ~118 ka, when the Mauca Llacta flow was

**Table 4** Sample data, including radiocarbon and calibrated ages, for Mina Arcata

Sample ID	Depth (cm)	Lab ID	Material	<sup>14</sup> C age	δ <sup>13</sup> C	Calibrated age
ARC-1-1A	393–395	OS-94467	Plant fragments	11,300 ± 45	–25.46	13,201 ± 100
ARC-1-1B	393–395	OS-94487	Plant fragments	11,400 ± 55	–19.18	13,266 ± 127
ARC-1-4	370	OS-94524	Plant fragments	8290 ± 66	–23.30	9278 ± 186
ARC-1-7	340	OS-94521	Plant fragments	7690 ± 50	–23.97	8492 ± 91

Radiocarbon dates calibrated to calendar years with OxCal v.4.2 (Ramsey 2009) and IntCal13 (Reimer et al. 2013)

emplaced. While we stress that this exposure age is a first-order estimate, due to the need for  $^3\text{He}$  production-rate calibration on this timescale (see below), this value aligns with unpublished  $^{40}\text{Ar}/^{39}\text{Ar}$  and U/Pb data from neighbouring flows (J-C Thouret, unpub. data). Following the LGM, a major effusive eruption deposited the NCF3 lava during the Late Glacial. A previous  $^{36}\text{Cl}$  age estimate placed this eruption  $\sim 8$  ka later, during the middle Holocene (sample NCNW28; Úbeda et al. 2012). That model conflicts with our data and with the glacial morphology and stratigraphy at this site, both of which suggest a Late Glacial age. Without knowing the full physical context of NCNW28, plausible explanations for its young age relative to COR-06-33 include post-depositional shielding by snow, ash and lapilli, which might reduce the cosmogenic ray flux to the sampled surface. Our data indicate emplacement of NCF1 and NCF2 occurred  $\sim 500$  years apart and prior to the most recent advance of Coropuna's ice cap. Acknowledging the minor age difference, we speculate that both flows were fed by  $175^\circ$  N-trending fissures along Coropuna's eastern flank, which intersected hydrothermal deposits of the eroded underlying edifice (Cerro Cuncaicha; Fig. 2a). We also posit that a thin ( $< 10$  cm), fine-grained black ashfall deposit, visible beneath the patchy soils on the massif's SSE–WSW flanks within  $\sim 20$  km of the vents, correlates with the two Holocene flows. Finally, we note that there is close agreement between our  $^3\text{He}$  ages from NCG1 and NCF2 and earlier  $^{36}\text{Cl}$  ages from the same landforms (Úbeda et al. 2012, 2018; Fig. 3a,b) and with the overlying glacial stratigraphy, all of which suggests the NCVC is active and not dormant as previously thought.

Two stratigraphically consistent  $^3\text{He}$  ages from the ASM confirm the middle-Holocene age of the Sabancaya edifice and lava field, in accord with previous estimates (Thouret et al. 1994, 1995b, 2001a; Samaniego et al. 2016). There is particularly close agreement between our helium age from the eastern basal unit (SBC-11-03:  $5.2 \pm 0.1$  ka) and previously published constraint for the western basal flow ( $5540 \pm 40$  cal yr BP), based on a  $^{14}\text{C}$  date of peat buried by a Holocene lava (Thouret et al. 2001b; Fig. 2b), although we acknowledge that these lavas are located on opposite sides of the volcano and not conclusively correlated. Compared with previously published  $^3\text{He}$  ages (Samaniego et al. 2016; recalculated in the same way as for our data), we note that while there is first-order similarity between our ages and their samples SA1 ( $6.0 \pm 0.3$  ka) and SA4 ( $6.6 \pm 0.3$  ka), there remains a conspicuous  $\sim 22\%$  offset in helium-3 concentrations (equivalent to  $\sim 1500$  years exposure age) between SBC-11-03 and SA4, despite both being from the same basal SA-3 flow. An even starker disparity exists with sample SA5 (Samaniego et al. 2016), also from the SA-3 flow, which gives an age ( $12.3 \pm 0.5$  ka) approximately twice as old as both samples SBC-11-03 and SA4. All three samples are from the same lava and thus should exhibit similar concentrations of

cosmogenic helium; yet, even accounting for intrinsic variability in lava composition and preparation and mass spectrometer sensitivity (typically 2%), we can offer no clear reason why three neighbouring samples give such divergent results. Without detailed information concerning the physical nature of samples SA4 and SA5, we must assume that both are erroneously old, potentially due to contamination by non-cosmogenic (e.g., magmatic)  $^3\text{He}$ . Consequently, our data refute the suggestion that Sabancaya's basal edifice was constructed during the Pleistocene–Holocene transition (Samaniego et al. 2016), a model founded on the older of the two disparate SA-3 helium ages.

Our  $^{36}\text{Cl}$  ages from the PDC and NC constitute the first chronologic data for either site. An exposure age of  $5.3 \pm 1.1$  ka from the south dome of the PDC indicates emplacement during the middle Holocene. On the basis of the relatively uniform degree of rock-surface weathering, this assignment potentially applies to the other domes in the complex, but full resolution of the PDC chronology will require extensive application of the  $^{36}\text{Cl}$  method. Meanwhile, the two  $^{36}\text{Cl}$  ages from NC provide preliminary constraints for two pulses of effusive volcanism during the middle-late Holocene. Similarly, basal  $^{14}\text{C}$  ages from the lava-dammed wetland in Quebrada Angostura provide the first-ever age constraint for the MA flow, which is tentatively correlated with the Arcata caldera (Thouret et al. 2016). Given that Late Pleistocene glacial till immediately underlies the organic-rich basal lacustrine sediments in this core, with no indication of an erosional unconformity, we suggest the average of two basal  $^{14}\text{C}$  ages (13.2 ka) is a closely limiting minimum age for eruption. Nonetheless, absolute dating control awaits  $^{10}\text{Be}$  surface-exposure dating of the lava itself.

Together, the voluminous lava flows and domes preserved at our five sites confirm the widespread occurrence of large, effusive eruptions during the Late Pleistocene and Holocene. At Coropuna, the copious volume of lava flows contrasts starkly with the small number of thin ashfall deposits and pumice layers from the same period (e.g., Thouret et al. 2002). While it is possible that pyroclastic deposits have been removed by subsequent subaerial and/or glacial erosion, such processes are not supported by prevailing climatic conditions or patterns of Late Pleistocene–Holocene glaciation (Bromley et al. 2011a,b; Úbeda et al. 2018), leading us to propose that volcanism at the NCVC has been defined by effusive volcanism since at least the last ice age. Our data confirm a comparable behaviour for Sabancaya (Samaniego et al. 2016), where  $> 80\%$  of the exposed lava area ( $\sim 60$  km<sup>2</sup>) can be assigned to the Holocene yet evidence for large explosive eruptions and pyroclastic deposition is absent. While it is too early to discount entirely the possibility of pyroclastic deposits associated with the PDC, NC, and MA eruptions, the preservation of voluminous lavas at these sites aligns with the NCVC and ASM and suggests a spatially extensive pattern

of effusive volcanism in SW Peru during the Late Pleistocene–Holocene. This finding highlights the need to (1) examine more carefully the evolution of lava flows in this part of the CVZ, where until now the focus has largely been on singular explosive eruptions (e.g., Huaynaputina) and ignimbrites, and (2) recognize the role of lava-forming eruptions lacking significant pyroclastic elements.

Our new data demonstrate that the NCV, like the neighbouring ASM, Nevado Chachani, and Volcán Misti, is an active magma system and thus a potential threat to human health and infrastructure. Unlike those volcanoes, the NCV currently supports the largest glacier in the tropics (~44 km<sup>2</sup> in 2015; Kochtitzky et al. 2018), raising the very real possibility of lahars in the event of renewed eruptions. Indeed, Úbeda et al. (2018) reported relict lahar deposits on the NE flank of the massif that they attribute to eruption of the NCF2, although these deposits have not been dated directly. While the existing lava chronology is insufficient to establish eruption rates at any of the five sites investigated here, the concomitance at Coropuna of extensive glaciation, active volcanism, and locally intensive human settlement emphasizes both the dearth of such information and the value in prioritizing high-resolution records for the glaciated CVZ. The potential hazard posed by the NCV in particular is an impetus for our ongoing geochronology efforts at that site.

In addition to establishing eruption recurrence and lava output rates for this under-studied region, the close stratigraphic relationship between volcanic and glacial deposits in SW Peru affords an invaluable opportunity for evaluating the role of (de)glaciation in magmatism. The debate into this potential relationship centres on Iceland; whether or not glacial loading/unloading impacts magma behaviour at convergent plate boundaries has not been tested. Within our data set, we note that both the MA and NCF3 lavas erupted during the Late Glacial period. Moreover, the occurrence of the latter soon after recession of Coropuna's ice cap is evidenced by a <sup>3</sup>He age (13.0 ka; recalculated from Bromley et al. (2009) using the same production rate and scaling for comparison) from a nearby glacial erratic boulder perched on the underlying glacial till (Fig. 3c). Yet, despite this apparently close timing, our database does not permit meaningful examination of glacial-magmatic links and we caution that temporal coincidence is weak evidence for causation. Our study does, however, demonstrate the feasibility of resolving the relative timing of cryospheric and volcanic behaviour on a site-by-site basis using a single method, thereby minimizing temporal uncertainties between the two records and helping identify lavas of glacial, deglacial, and post-glacial age. Such lavas can then be used as targets for geochemical assessment of magma production, storage, and remobilisation (e.g., Cooper and Kent 2014) in the context of cryospheric change.

Methodologically, our lava chronology from SW Peru supports the use of cosmogenic nuclides for direct dating of Late

Pleistocene–Late Holocene-age lavas, timescales that are relevant for estimating long-term eruption rates in SW Peru and more broadly. Application of the stable nuclide <sup>3</sup>He to older (e.g., Pliocene) lavas is theoretically possible but depends on the degree of post-depositional surface erosion, which can be considerable even under prevailing arid conditions. Our oldest-dated flow, NCF4, illustrates how <sup>3</sup>He dating can be combined effectively with other geochronologic methods, such as U/Pb, both as a means of cross-checking cosmogenic data and for filling gaps in the record where one method is compromised (e.g., due to surface erosion). At the same time, NCF4 underscores the need to calibrate cosmogenic nuclide production rates on volcanically relevant timescales. The majority of production rate estimates currently in use are calibrated against landforms < 20 ka in age (see Borchers et al. 2016), and while our age for NCF4 assumes this rate has remained broadly constant over time, there is considerable debate within the scientific community as to the validity of this assumption. The impact of geomagnetic variability on the cosmic ray flux, for example, is unconstrained yet has potentially significant ramifications for terrestrial cosmogenic nuclide production on long timescales (see Lifton et al. 2014; Online Resource 1). Going forward, the coupling of cosmogenic nuclide dating with methods such as <sup>40</sup>Ar/<sup>39</sup>Ar and U/Pb affords a foundation not only for constraining lava age but also for calibrating cosmogenic nuclide production on numerous relevant timescales and thus must be prioritized.

## Conclusions

Eight cosmogenic <sup>3</sup>He and three <sup>36</sup>Cl ages, along with new minimum-limiting <sup>14</sup>C dates, document multiple episodes of effusive volcanism in the Andes of southern Peru over the past ~ 118 ka, including two Late Holocene events on the NCV. Our <sup>3</sup>He and <sup>36</sup>Cl data, inferred from measurements in pyroxene and feldspar separates, respectively, demonstrate that cosmogenic surface-exposure dating is an effective tool for reconstructing volcanic activity in the Western Cordillera, particularly for young (and potentially historic) lavas that are beyond the scope of traditional geochronologic methods yet crucial for establishing the timing and frequency of recent eruptions. In our study area, the prevailing semi-arid climate maintains a high degree of surface preservation and minimizes potential complicating factors, such as shielding by snow and vegetation. Furthermore, the analytical resolution of the surface-exposure toolset is approaching the point at which meaningful comparisons with other chronologies become possible and, critically, the potential relationships between magma generation/storage and geomorphic–climatic processes, such as cryospheric change and edifice collapse, might be established effectively.

Acknowledging the exciting potential of cosmogenic surface-exposure dating for volcanic applications on both very young and very old timescales, we stress that limitations in our current understanding of nuclide production rates, and how they might vary over time, remain an important source of methodological uncertainty. This is particularly true for the Tropics, where the magnitude of geomagnetic variance is greatest, and highlights the need for renewed calibration efforts over a broad range of timescales.

**Acknowledgements** We thank Claire Todd and Matthew Hegland (Pacific Lutheran University), Rigoberto Aguilar (OVI Ingemmet, Arequipa), and Peter Strand (UMaine) for field and sampling assistance. We also thank Mark Kurz and Josh Curtice, Woods Hole Oceanographic Institute, for input during sample preparation and helium measurement. Pierre Boivin, Claire Fonquernie, Mhammed Benbakkar, and Jean-Luc Davidal provided analytical laboratory assistance. G. Bromley acknowledges support from NSF grant EAR-10-03427 and the Churchill Exploration Foundation (UMaine). The ASTER AMS national facility (CEREGE, Aix en Provence) is supported by the INSU/CNRS, the ANR through the 'Projets thématiques d'excellence' programme for the 'Equipements d'excellence' ASTER-CEREGE action and IRD. Finally, we extend our thanks to Jorge Vasquez, an anonymous reviewer, Associate Editor Hannah Dietterich and Editor Jacopo Taddeucci for their thoughtful and constructive comments on earlier versions of this manuscript. CLERVOLC and I-SITE contribution 356. Consortium: Georges Aumaître, Didier Bourlès, Karim Keddadouche

## References

- Alcalá J, Estremera DP, Zamorano JJ, Vázquez-Selem L (2011) Last glacial maximum and deglaciation of Ampato volcanic complex, Southern Peru. *Cuaternario y geomorfología: Revista de la Sociedad Española de Geomorfología y Asociación Española para el Estudio del Cuaternario* 25:121–136
- Alcalá Reygosa J, Palacios D, Zamorano Orozco JJ (2016) Geomorphology of the Ampato volcanic complex (southern Peru). *J Maps* 12:1160–1169
- Alcalá-Reygosa J, Arce JL, Schimmelpfennig I, Salinas EM, Rodríguez MC, Léanni L, Aumaître G, Bourlès D, Keddadouche K, Team ASTER (2018) Revisiting the age of the Jumento volcano, Chichinautzin volcanic field (Central Mexico), using in situ-produced cosmogenic  $^{10}\text{Be}$ . *J Volcan Geotherm Res* 366:112–119
- Allmendinger RW, Jordan TE, Kay SM, Isacks BL (1997) The evolution of the Altiplano-Puna plateau of the central Andes. *Ann Rev Earth Plan Sci* 25:139–174
- Andronico D, Lodato L (2005) Effusive activity at Mount Etna volcano (Italy) during the 20th century: a contribution to volcanic hazard assessment. *Nat Haz* 36:407–443
- Baker MCW (1981) The nature and distribution of upper cenozoic ignimbrite centres in the Central Andes. *J Volcanol Geotherm Res* 11: 293–315
- Blard PH, Lavé J, Sylvestre F, Placzek CJ, Claude C, Galy V, Condom T, Tibari B (2013) Cosmogenic  $^3\text{He}$  production rate in the high tropical Andes (3800 m, 20°S): implications for the local last glacial maximum. *Earth Plan Sci Lett* 377–378:260–275
- Borchers B, Marrero S, Balco G, Caffee M, Goehring B, Lifton N, Nishiizumi K, Phillips F, Schaefer J, Stone J (2016) Geological calibration of spallation production rates in the CRONUS-earth project. *Quat Geochronol* 31:188–198
- Bromley GRM, Schaefer JM, Winckler G, Hall BL, Todd CE, Rademaker KM (2009) Relative timing of last glacial maximum and late-glacial events in the central tropical Andes. *Quat Sci Rev* 28:2514–2526
- Bromley GR, Hall BL, Rademaker KM, Todd CE, Racoviteanu AE (2011a) Late Pleistocene snowline fluctuations at Nevado Coropuna (15 S), southern Peruvian Andes. *J Quat Sci* 26:305–317
- Bromley GRM, Hall BL, Schaefer JM, Winckler G, Todd CE, Rademaker KM (2011b) Glacier fluctuations in the southern Peruvian Andes during the late-glacial period, constrained with cosmogenic  $^3\text{He}$ . *J Quat Sci* 26:37–43
- Bulmer M, Johnston A, Engle F (1999) Analysis of Sabancaya volcano, southern Peru using Radarsat and Landsat TM data. Application Development and Research Opportunity (ADRO)
- Burkett B (2008) Andean volcanism: Nevado Hualca Hualca volcano, Southern Peru, and El Reventador Volcano, Ecuador. Unpublished M.S. thesis, SUNY Buffalo
- Clapperton CM (1993) Quaternary geology and geomorphology of South America. Elsevier. 779 pp
- Cobeñas G, Thouret JC, Bonadonna C, Boivin P (2014) Reply to comment on: "Cobeñas, G., Thouret, J.-C., Bonadonna, C., Boivin, P., 2012. The c.2030 yr BP Plinian eruption of El Misti volcano, Peru: eruption dynamics and hazard implications". *J Volcanol Geotherm Res* 275C:103–113
- Cooper KM, Kent AJ (2014) Rapid remobilization of magmatic crystals kept in cold storage. *Nature* 506:480–483
- Delacour A, Gerbe MC, Thouret JC, Wörner G, Paquereau-Lebti P (2007) Magma evolution of quaternary minor volcanic centres in southern Peru, Central Andes. *Bull Volcanol* 69:581–608
- Dorbath C (1996) Velocity structure of the Andes of central Peru from locally recorded earthquakes. *Geophys Res Lett* 23:205–208
- Forget M, Thouret JC, Kuentz A, Fontugne M (2008) Héritages glaciaires, périglaciaires et évolution récente: le cas du Nevado Coropuna (Andes centrales, sud du Pérou). *Géomorphologie: Relief, Processus, Environnement* 2:113–132
- Francis PW, Hawkesworth CJ (1994) Late Cenozoic rates of magmatic activity in the central Andes and their relationship to continental crust formation and thickening. *J Geol Soc Lond* 151:845–854
- Gehrels MJ, Lowe DJ, Hazell ZJ, Newnham RM (2006) A continuous 5300-yr Holocene cryptotephrostratigraphic record from northern New Zealand and implications for tephrochronology and volcanic hazard assessment. *The Holocene* 16:173–187
- Gerbe MC, Thouret JC (2004) Role of magma mixing in the petrogenesis of tephra erupted during the 1990–98 explosive activity of Nevado Sabancaya, southern Peru. *Bull Volcanol* 66:541–561
- Gunnell Y, Thouret JC, Bricchau S, Carter A, Gallagher K (2010) Low-temperature thermochronology in the Peruvian Central Andes: implications for long-term continental denudation, timing of plateau uplift, canyon incision and lithosphere dynamics. *J Geol Soc* 167: 803–815
- Hall K (1982) Rapid deglaciation as an initiator of volcanic activity: an hypothesis. *Earth Surface Proc Land* 7:45–51
- Harðarson BS, Fitton JG (1991) Increased mantle melt beneath Snaefellsjökull volcano during Late Pleistocene deglaciation. *Nature* 353:62–64
- Herreros J, Moreno I, Taupin JD, Ginot P, Patris N, De Angelis M, Ledru MP, Delachaux F, Schotterer U (2009) Environmental records from temperate glacier ice on Nevado Coropuna saddle, southern Peru. *Adv Geosci* 7:1–8
- Hooper A, Ófeigsson B, Sigmundsson F, Lund B, Einarsson P, Geirsson H, Sturkell E (2011) Increased capture of magma in the crust promoted by ice-cap retreat in Iceland. *Nat Geosci* 4:783–786
- Hora JM, Singer BS, Wömer G (2007) Volcano evolution and eruptive flux on the thick crust of the Andean central volcanic zone:

- $^{40}\text{Ar}/^{39}\text{Ar}$  constraints from Volcán Parínacota, Chile. *GSA Bull* 119: 343–362
- Huaman-Rodrigo D, Chorowicz J, Deffontaines B, Guillaude R, Rudant JP (1993) Cadre structural et risques géologiques étudiés à l'aide de l'imagerie spatiale: la région du Colca (Andes du sud Pérou). *Bull Société Géologique France* 164:807–818
- Huybers P, Langmuir C (2009) Feedback between deglaciation, volcanism, and atmospheric  $\text{CO}_2$ . *Earth Plan Sci Lett* 286:479–491
- James DE (1971) Plate tectonic model for the evolution of the Central Andes. *Geol Soc Am Bull* 82:3325–3346
- Juvigné E, Thouret JC, Gilot E, Gourgaud A, Graf K, Legros F, Uribe M (1997) Etude téphrostratigraphique et bioclimatique du Tardiglaciaire et de l'Holocène de la Laguna Salinas, Pérou méridional. *Géographie Phys Quat* 51:221–233
- Juvigné E, Thouret JC, Loutsch I, Lamadon S, Frechen M, Fontugne M, Rivera M, Da Vila J, Mariño J (2008) Retombées volcaniques dans des tourbières et lacs autour du massif des Nevados Ampato et Sabancaya (Pérou Méridional, Andes Centrales). *Quaternaire* 19: 157–173
- Kelly MA, Lowell TV, Applegate PJ, Phillips FM, Schaefer JM, Smith CA, Kim H, Leonard KC, Hudson AM (2015) A locally calibrated, late glacial 10Be production rate from a low-latitude, high-altitude site in the Peruvian Andes. *Quat Geochron* 26:70–85
- Kochitzky WH, Edwards BR, Enderlin EM, Marino J, Marinque N (2018) Improved estimates of glacier change rates at Nevado Coropuna Ice Cap, Peru. *J Glaciol* 64:175–184
- Lal D (1991) Cosmic ray labeling of erosion surfaces: in situ nuclide production rates and erosion models. *Earth Plan Sci Lett* 104:424–439
- Lamadon S (1999) Fluctuations glaciaires et téphrostratigraphie dans les montagnes intertropicales : une revue et application dans les Andes du Sud Pérou (massifs des Nevados Ampato et Coropuna). Mémoire de DEA (non publié), Université Blaise Pascal, 180 p
- Lentfer C, Torrence R (2007) Holocene volcanic activity, vegetation succession, and ancient human land use: unraveling the interactions on Garua Island, Papua New Guinea. *Rev Palaeobot Palynol* 143:83–105
- Lifton N, Sato T, Dunai TJ (2014) Scaling in situ cosmogenic nuclide production rates using analytical approximations to atmospheric cosmic-ray fluxes. *Earth Plan Sci Lett* 386:149–160
- Maclennan J, Jull M, McKenzie D, Slater L, Grönvold K (2002) The link between volcanism and deglaciation in Iceland. *Geochem Geophys Geosyst* 3:1–25
- Mark BG, Seltzer GO (2005) Glacier recession in the Peruvian Andes: Climatic forcing, hydrologic impact and comparative rates over time. In *Global Change and Mountain Regions* (pp. 205–214). Springer Netherlands
- Marrero SM, Phillips FM, Caffee MW, Gosse JC (2016) CRONUS-earth cosmogenic  $^{36}\text{Cl}$  calibration. *Quat Geochron* 31:199–219
- Martin LCP, Blard PH, Balco G, Lavé J, Delunel R, Lifton N, Laurent V (2017) The CREP program and the ICE-D production rate calibration database: a fully parameterizable and updated online tool to compute cosmic-ray exposure ages. *Quat Geochron* 38:25–49
- Molloy C, Shane P, Augustinus P (2009) Eruption recurrence rates in a basaltic volcanic field based on tephra layers in maar sediments: implications for hazards in the Auckland volcanic field. *GSA Bull* 121:1666–1677
- Nowell DAG, Jones MC, Pyle DM (2006) Episodic quaternary volcanism in France and Germany. *J Quat Sci* 21:645–675
- Pagli C, Sigvaldson F (2008) Will present day glacier retreat increase volcanic activity? Stress induced by recent glacier retreat and its effect on magmatism at the Vatnajökull ice cap, Iceland. *Geophys Res Lett* 35:L09304. <https://doi.org/10.1029/2008GL033510>
- Ramsey CB (2009) Bayesian analysis of radiocarbon dates. *Radiocarbon* 51:337–360
- Reimer PJ, Bard E, Bayliss A, Beck JW, Blackwell PG, Ramsey CB, Buck CE, Cheng H, Edwards RL, Friedrich M, Grootes PM (2013) IntCal13 and Marine13 radiocarbon age calibration curves 0–50,000 years cal BP. *Radiocarbon* 55:1869–1887
- Samaniego P, Barba D, Robin C, Fornari M, Bernard B (2012) Eruptive history of Chimborazo volcano (Ecuador): a large, ice-capped and hazardous compound volcano in the Northern Andes. *J Volcanol Geotherm Res* 221:33–51
- Samaniego P, Rivera M, Mariño J, Guillou H, Liorzou C, Zerathe S, Delgado R, Valderrama P, Scao V (2016) The eruptive chronology of the Ampato–Sabancaya volcanic complex (Southern Peru). *J Volcanol Geotherm Res* 323:110–128
- Schimmelfennig I, Benedetti L, Finkel R, Pik R, Blard PH, Bourlès D, Burnard P, Williams A (2009) Sources of in-situ  $^{36}\text{Cl}$  in basaltic rocks. Implications for calibration of production rates. *Quat Geochron* 4: 441–461
- Schimmelfennig I, Benedetti L, Garreta V, Pik R, Blard PH, Burnard P, Bourlès D, Finkel R, Ammon K, Dunai T (2011) Calibration of cosmogenic  $^{36}\text{Cl}$  production rates from Ca and K spallation in lava flows from Mt. Etna (38°N, Italy) and Payun Matru (36°S, Argentina). *Geochim Cosmochim Acta* 75:2611–2632
- Schimmelfennig I, Schaefer J, Putnam A, Koffman T, Benedetti L, Ivy-Ochs S, ASTER Team, Schlüchter C (2014)  $^{36}\text{Cl}$  production rate from K-spallation in the European Alps (Chironico landslide, Switzerland). *J Quat Sci* 29:407–413
- Siebe C, Arana-Salinas L, Abrams M (2005) Geology and radiocarbon ages of Tlalóc, Tlacotenco, Cuauhtzin, Hijo del Cuauhtzin, Teuhtli, and Ocusacayo monogenetic volcanoes in the central part of the Sierra Chichinautzin, México. *J Volcanol Geotherm Res* 141:225–243
- Stern CR (2004) Active Andean volcanism: its geologic and tectonic setting. *Revista Geol Chile* 31:161–206
- Stone JO (2000) Air pressure and cosmogenic isotope production. *J Geophys Res* 105(B10):23753–23759
- Thouret JC, Cantagrel JM, Salinas R, Murcia A (1990) Quaternary eruptive history of Nevado del Ruiz (Colombia). *J Volcanol Geotherm Res* 41:225–251
- Thouret JC, Guillaude R, Huaman D, Gourgaud A, Salas G, Chorowicz J (1994) L'activité actuelle du Nevado Sabancaya (Sud Pérou): reconnaissance géologique et satellitaire, évaluation et cartographie des menaces volcaniques. *Bull Soc Géol France* 165:49–63
- Thouret JC, Cantagrel JM, Robin C, Murcia A, Salinas R, Cepeda H (1995a) Quaternary eruptive history and hazard-zone model at Nevado del Tolima and Cerro Machin volcanoes, Colombia. *J Volcanol Geotherm Res* 66:397–426
- Thouret JC, Gourgaud A, Uribe M, Rodriguez A, Guillaude R, Salas G (1995b) Geomorphological and geological survey, and SPOT remote sensing of the current activity of Nevado Sabancaya stratovolcano (Peru): assessment for hazard-zone mapping. *Zeit Geomorph* 39(4):515–535
- Thouret JC, Finizola A, Fornari M, Legeley-Padovani A, Suni J, Frechen M (2001a) Geology of El Misti volcano nearby the city of Arequipa, Peru. *GSA Bull* 113:1593–1610
- Thouret JC, Juvigné E, Loutsch I, Chavez Chavez JA (2001b) Historic volcanic activity and human sacrifices by the Incas in Southern Peru. In: Juvigné E, Raynal J-P (eds) *Tephros: chronology, archaeology*. *Dossiers de 14Archéo-Logis*, pp 219–226
- Thouret JC, Juvigné E, Mariño J, Moscol M, Legeley-Padovani A, Loutsch I, Davila J, Lamadon S, Rivera M (2002) Late Pleistocene and Holocene tephro-stratigraphy and chronology in southern Peru. *Bol Soc Geol Perú* 93:45–61
- Thouret JC, Davila J, Juvigné E, Lee A, Legeley-Padovani A, Loutsch I, Majavesi M, Jersey M, Moscol M (2003) Late Pleistocene and Holocene tephrostratigraphy and chronology in southern Peru. XVI INQUA Congress, pp 23–30

- Thouret JC, Rivera M, Wörner G, Gerbe MC, Finizola A, Fornari M, Gonzales K (2005) Ubinas: the evolution of the historically most active volcano in southern Peru. *Bull Volcanol* 67:557–589
- Thouret JC, Jicha B, Paquette JL, Cubukcu E (2016) A 25 Myr chronostratigraphy of ignimbrites in South Peru. Implications for the volcanic history of the Central Andes. *J Geol Soc* 173:734–756
- Thouret JC, Gunnell Y, Jicha B, Paquette JL, Braucher R (2017) Evolution and river incision history of the west Central Andes based on ignimbrites, landslide study and surface exposure dating in SW Peru. *Geomorph* 298:1–19
- Úbeda J, Palacios D, Vázquez-Selem L (2012) La evolución glaciovolcánica del nevado Coropuna desde la transición del Pleistoceno al Holoceno. In: XVI Congreso Peruano de Geología. Soc Geol Perú, Lima
- Úbeda J, Bonshoms M, Iparraguirre J, Sáez L, De la Fuente R, Janssen L, Concha R, Vásquez P, Masías P (2018) Prospecting glacial ages and Paleoclimatic reconstructions Northeastward of Nevado Coropuna (16°S, 73°W, 6377 m), arid tropical Andes. *Geosci* 8:307
- Venturelli G, Frangipane M, Weibel M, Antiga D (1978) Trace element distribution in the Cainozoic lavas of Nevado Coropuna and Andagua Valley, Central Andes of southern Peru. *Bull Volcanol* 41–43:213–228
- Vuille M, Francou B, Wagnon P, Juen I, Kaser G, Mark BG, Bradley RS (2008) Climate change and tropical Andean glaciers: past, present and future. *Earth Sci Rev* 89:79–96
- Weibel VM, Frangipane-Gysel M, Hunziker J (1978) Ein Beitrag zur Vulkanologie Süd-Perus. *Geol Rundsch* 67:243–252
- Wörner G, Hammerschmidt K, Henjes-Kunst F, Lezaun J, Wilke H (2000) Geochronology ( $^{40}\text{Ar}/^{39}\text{Ar}$ , K-Ar and He-exposure ages) of Cenozoic magmatic rocks from Northern Chile (18–22°S): implications for magmatism and tectonic evolution of the central Andes. *Revista Geol Chile* 27:205–240
- Wörner G, Mamani M, Blum-Oeste M (2018) Magmatism in the Central Andes. *Elements* 14(4):237–244